Period-adding route in sparkling bubbles

Gérard Liger-Belair,[1,*] Alberto Tufaile,[2,3] Bertrand Robillard,[4] Philippe Jeandet,[1] and José Carlos Sartorelli[2]
[1]*Laboratoire d'oenologie et de Chimie Appliquée, UPRES EA 2069, URVVC, Faculté des Sciences de Reims, Moulin de la Housse, B.P. 1039, 51687 Reims, Cedex 2, France*
[2]*Instituto de Física, Universidade de São Paulo, Caixa Postal 66318, 05315-970, São Paulo, SP, Brazil*
[3]*Escola de Artes, Ciências e Humanidades, Universidade de São Paulo, Caixa Postal 66318, 03828-000, São Paulo, SP, Brazil*
[4]*M&C, Laboratoire de Recherches, 6 rue Croix de Bussy, 51200 Epernay, France*
(Received 21 February 2005; published 13 September 2005)

Chains of bubbles are seen rising along the wall whenever champagne is poured into a glass. The careful observation of a given bubble chain often reveals that the interbubble distance suddenly changes during the degassing process, indicating different bubbling regimes in this elusive phenomenon of effervescence. We report the transitions between these different bubbling regimes that present sequences of multiple periods known as the period-adding route.

DOI: 10.1103/PhysRevE.72.037204 PACS number(s): 05.45.−a, 47.52.+j, 83.60.Wc

Instabilities leading to transitions in effervescent systems are observed from biological systems to the food industry [1,2]. A striking example of the influence of transitions in degassing process is the dangerous behavior of the explosive release of CO_2 from lake Nyos [3]. Moreover, the main cause of an embolism in living beings also involves bubble formation from liquids supersaturated with dissolved gas. For example, gas bubbles can nucleate and develop in the xylem, the water conducting tissue of vascular plants, which leads to a blockage of water transport [4]. A gas embolism may also arise in divers who have breathed high-pressure air, if they resurface too quickly [5].

Our experiment focuses on the dynamics of bubble nucleation from the wall of a glass freshly poured with champagne. In this paper we report that the multiperiodic bubbling dynamics from sparkling bubbles undergo sequences known as a period-adding route, similar to those observed in the complex response in neurons, rhythmic processes in physiology, electronic circuits, ocean wave motion, and bubble columns [6–10].

The close-up examination of an everyday situation like the fizzing of champagne revealed a curious and unexpected phenomenon. Actually, chains of bubbles are seen rising along the wall whenever champagne is poured into a glass. In Fig. 1, macrophotographs of a typical bubble chain issued from a given bubble nucleation site followed with time while degassing are displayed. It is observed that the bubbling regime changes in time. In Fig. 1(A) bubbles are seen generated from a period-2 bubbling regime, which is characterized by the fact that two successive bubbles rise in pairs. Later, a multiperiodic bubbling regime arises, which is displayed in Fig. 1(B). Then a bubbling in period 3 occurs and is shown in Fig. 1(C). Finally, the nucleation site ends in a clockwork period-1 bubbling regime presented in Fig. 1(D), where the distance between two successive bubbles increases monotonically as they rise. Thus, a transition from multiperiodic to a clockwork period-1 bubbling regime takes place, raising the question of what mechanism will be responsible for the transitions between the different bubbling regimes.

In weakly carbonated water solutions, the clockwork period-1 bubbling from a cavity of the vessel's surface has already been reported and interpreted by Jones *et al.* [11]. The authors of the previous work proposed two characteristic time scales for the cycle of bubble production: (*i*) the bubble growth time, denoted t_g and (*ii*) the bubble nucleation time, denoted t_n. t_g is the time required for a bubble, being rooted to its nucleation site by capillary forces, to grow by diffusion to its detachment size, whereas t_n is the time lapse between the moment the bubble detaches from the site and the moment a new bubble reappears at the same site. In this model, the time interval between two successive bubbles is the total time per cycle, i.e., $T=t_g+t_n$. Consequently, the bubbling frequency of a given nucleation site is defined as $F_b=1/T$.

The dynamics of sparkling bubbles is nevertheless quite different than the previous description accounting, only for the clockwork period-1 bubbling regime. Actually, most of the bubble nucleation sites in carbonated beverages were recently identified as being located on bubble embryos trapped inside tiny and roughly cylindrical hollow cellulose-fiber structures of the order of 100 μm, with a cavity mouth of a few micrometers [12]. The close-up observation (conducted *in situ* from high-speed video camera recordings) revealed that the gas pocket trapped inside the fiber oscillates with its own frequency F_c higher than the bubbling frequency F_b (see Fig. 2). The hollow cavity inside the fiber where the trapped bubble embryo oscillates is denoted the *lumen*. It is also worth noting that, in comparison with other types of bubbling from artificial nozzles or boiling systems [10,13–15] bubbles ejected from these tiny cellulose fibers present the more spherical shapes observed, due to their very low Weber numbers close to the fiber tip.

Actually, $\mathrm{We}=(2\rho R U^2)/\gamma \approx 10^{-6}-10^{-5} \ll 1$, where We, R, U, ρ, and γ are the Weber number, the bubble radius, the bubble velocity, the liquid density, and its surface tension, respectively.

Two different and well-defined oscillators may be distin-

*Corresponding author. Electronic address: gerard.liger-belair@univ-reims.fr

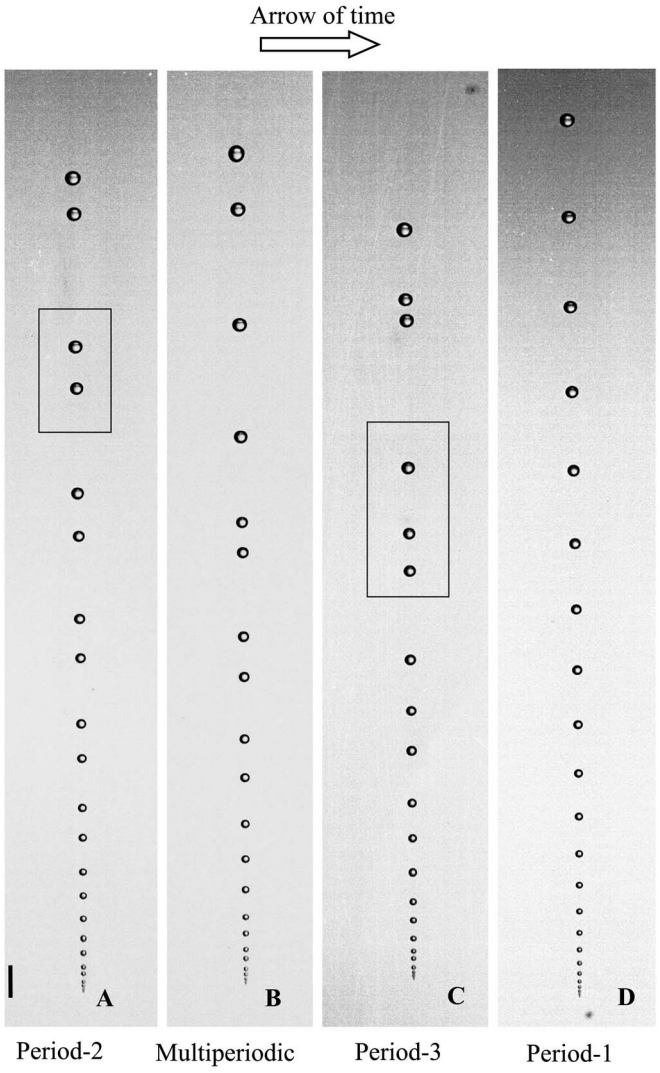

FIG. 1. (a)–(d) Macrophotographs of the bubble chain issued from a given nucleation site on the wall of a glass poured with champagne. As time proceeds, the bubble nucleation site experiences different bubbling regimes; in (A) bubbles are seen generated from a period-2 bubbling regime, which is characterized by the fact that two successive bubbles rise in pairs. (B) Multiperiodic bubbling. As time passes, a bubbling in period 3 occurs and is shown in (C). Finally, after others various changes in the bubbling regime, the nucleation site ends in a clockwork period-1 bubbling regime shown in (D) (bar=1 mm).

guished in this tiny bubbling system [see Fig. 3(a)]: (i) the gas pocket oscillating while trapped inside the fiber's lumen, and (ii) the released bubble in touch with the tip of the fiber. In what follows, we analyze both oscillators independently.

(i) The characteristic time required for a period of the oscillating trapped gas pocket is accessible by applying the classical Fick's law to the CO_2 molecules that diffuse from the liquid bulk into the gas pocket through the gas/liquid interface. This period is accessible by evaluating the time needed for a gas pocket to grow, from its initial position to the tip of the fiber. Actually, the cellulose fiber was considered as a nearly cylindrical microchannel, where the trapped gas pocket grows by diffusion. The following equation was derived for approaching the period of the gas pocket oscillation:

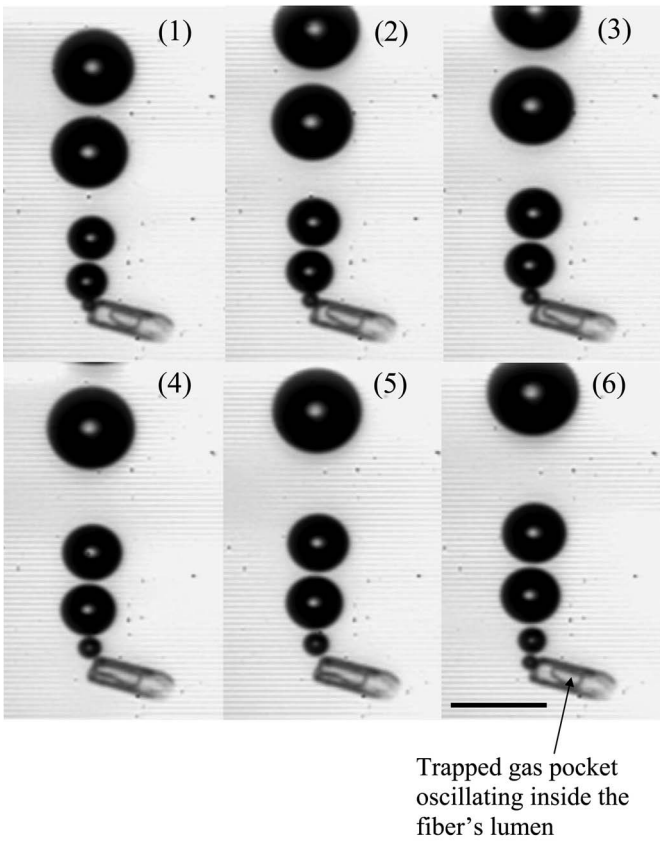

FIG. 2. Close-up time-sequence illustrating one period of the oscillation of the gas pocket trapped inside the fiber's lumen. The nucleation site is in its period-2 bubbling regime. The time interval between two successive frames is 20 ms (bar=50 μm).

$$t_n \approx \frac{\left(P_0 + \frac{2\gamma}{r}\right)}{\Re\theta D}\frac{\lambda h}{\Delta c}, \tag{1}$$

where P_0 is the atmospheric pressure, γ the liquid surface tension, D the diffusion coefficient of CO_2 molecules through the liquid medium, r the inner radius of the fiber, $\Re$ the ideal gas constant, θ the absolute temperature, h the course of the gas pocket oscillation [see Fig. 3(a)], and λ the boundary layer around the gas/liquid interface where a gradient Δc of dissolved-CO_2 molecules exists.

Finally, the frequency F_c of the oscillating gas pocket is approached by

$$F_c \approx \frac{1}{t_n} \approx \frac{\Re\theta D}{\left(P_0 + \frac{2\gamma}{r}\right)}\frac{\Delta c}{\lambda h}. \tag{2}$$

(ii) The bubble, which is blown by the fiber, does not anchor to the fiber tip (because of unfavorable wetting conditions). Actually, the cellulose is highly hydrophilic and forbids any contact line. Therefore, the released bubble immediately begins its rise through the liquid. In the very few tens

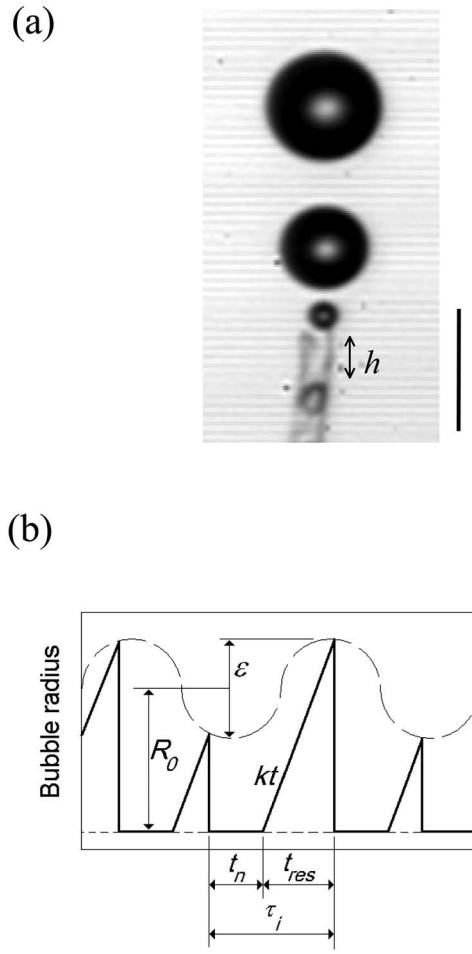

FIG. 3. The cellulose fiber blowing bubbles is a tiny "bubble gun" modeled as a system of two coupled oscillators; the course of the bubble embryo oscillating trapped inside the fiber's lumen is denoted h (bar=50 μm) (a). Temporal evolution obtained from the model for a period-2 bubbling regime, in which the bubble radius function has a threshold given by an envelope $\varepsilon\cos(2\pi\Omega F_b\tau)$ (b).

of micrometers of its early rise, the Reynolds number of the bubble is much lower than unity and its velocity of rise U is close to the well-known Stokes velocity, $U=(2\rho g R^2)/9\eta$, where R is the bubble radius, ρ the liquid density, η the liquid viscosity, and g the acceleration due to gravity [12].

However, while rising through the liquid supersaturated with dissolved gas, the bubble still continues to grow by diffusion with a constant growth rate, $k=dR/dt$ [12]. The absolute velocity of the rear part of the bubble is therefore the sum of the velocity of the center of mass of the bubble U (pointing upward) and the velocity of the rear part of the bubble k (pointing downward). Consequently, the released bubble stays in touch with the tip of the fiber as soon as k is higher than the Stokes velocity U. The critical radius needed to leave the tip of the fiber is therefore accessible through

$$U=\frac{2\rho g}{9\eta}R^2 \geqslant k \Rightarrow R_C=\sqrt{\frac{9\eta k}{2\rho g}}. \tag{3}$$

The characteristic time needed to reach this critical size for a bubble is denoted the residence time t_{res}, and may be estimated from the relation

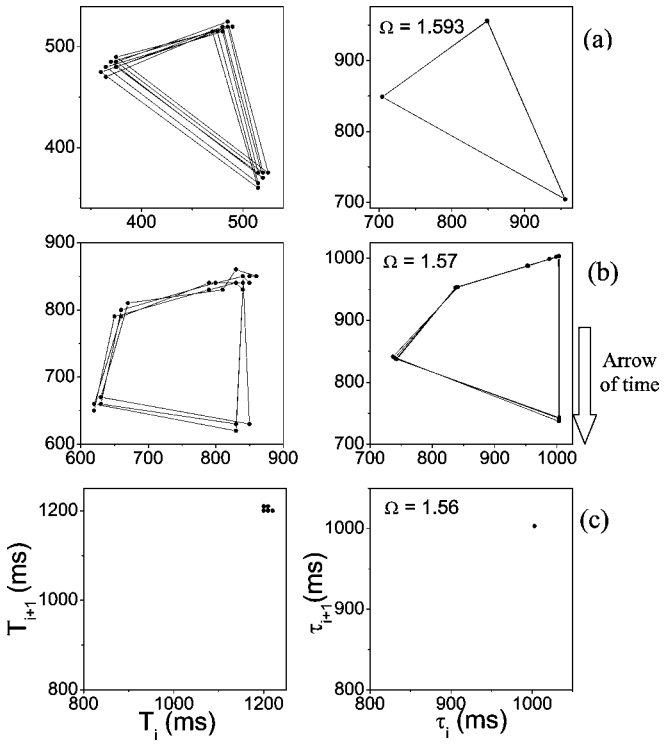

FIG. 4. A comparison between attractors obtained from the experiment (left) and from the model (right), respectively; the lines between successive dots show the cycle; in (a) the bubbling regime is in a period 3; in (b) there is a pile-up when the points come into the vicinity of $T=850$ ms, and a very similar behavior is obtained with the model for a period-7 bubbling regime; in (c) the system ends abruptly in a clockwork period-1 bubbling regime. The bubbling dynamics, both in the experiment and in the model, are characterized by a sequence of increasing periodicity always ending in a clockwork period-1 bubbling regime.

$$k=\frac{dR}{dt}\approx\frac{R_C}{t_{res}}\Rightarrow t_{res}\approx\frac{R_C}{k}\approx\sqrt{\frac{9\eta}{2\rho g k}}. \tag{4}$$

The bubble growth rate k during the bubble rise has been derived in a previous paper [12], where it was connected with some parameters of the liquid medium as follows:

$$k=\frac{dR}{dt}\approx 0.63\frac{\Re\theta}{P_0}D^{2/3}\left(\frac{2\rho g}{9\eta}\right)^{1/3}\Delta c. \tag{5}$$

Finally, the total time required for a bubble to definitively leave the fiber's tip is $T=t_n+t_{res}$. Consequently, the bubbling frequency F_b may be written as

$$F_b=\frac{1}{T}=\frac{1}{t_n+t_{res}}. \tag{6}$$

The control parameter Ω that was chosen as the ratio between F_c and F_b may then be written as follows:

$$\Omega=\frac{F_c}{F_b}=\frac{t_n+t_{res}}{t_n}=1+\frac{t_{res}}{t_n}. \tag{7}$$

By replacing in the latter equation the values of t_n and t_{res} defined in Eqs. (1) and (4), the theoretically derived relation-

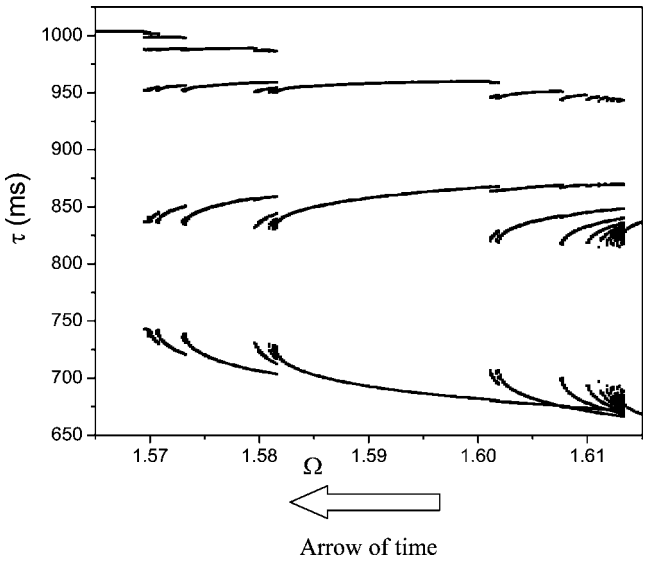

FIG. 5. Bifurcation diagram of stable periodic points obtained by numerical simulation and by gradually decreasing the frequency ratio Ω.

ship for the bubble growth rate k defined in (5), the control parameter Ω may be connected with both some fluid and fiber parameters as follows:

$$\Omega \approx 1 + A(\Delta c)^{1/2},$$

$$\text{with } A \approx \left(\frac{9\eta}{2\rho g}\right)^{2/3} \frac{P_0^{1/2} D^{2/3} (\Re\theta)^{1/2}}{\left(P_0 + \frac{2\gamma}{r}\right)\lambda h}. \tag{8}$$

As time proceeds during the continuously bubbling process, the only parameter that gradually changes in (8) is the concentration of dissolved CO_2 molecules through Δc.

The envelope in the bubble radius function, shown in Fig. 3(b), represents the influence of the trapped gas pocket (which oscillates at a frequency $F_c = \Omega F_b$), given by $\varepsilon \cos(2\pi\Omega F_b \tau)$. The parameter ε is related to the amplitude of interactions between the two systems, and in the model the value is $\varepsilon = (t_n + t_{res})/5$. This value was inferred from observations made from the experiments, in which t_{res} is the residence time without the influence of the gas pocket. Therefore, the residence time and the oscillatory motion of the gas pocket control the bubble radius $R(\tau)$. The bubbling mode is given by

$$R(\tau_{i+1}) = R_0 + \varepsilon \cos(2\pi\Omega F_b \tau_{i+1}),$$

$$\tau_i = t_n + t_{res}, \tag{9}$$

where R_0 is the radius of the bubble just blown from the fiber's tip, and τ_i is the time interval between two successive bubbles.

By using Ω as the control parameter, we obtained some attractors that can be compared with the experimental reconstructed attractors. Numerous nucleation sites were followed while degassing. Series of time intervals departure T_i between successive bubbles were taken, all along the degassing process, and plotted as a function of one another (T_{i+1} vs T_i). For a given nucleation site, Figs. 4(a)–4(c) present a comparison between some maps obtained from the experiment (left) and from the model (right), respectively. Figure 5 shows the bifurcation diagram of stable periodic points obtained by numerical simulation and by gradually decreasing the frequency ratio Ω. The bifurcation has the same characteristics of systems that present a sequence known as period-adding route [6–10]. The period-adding scenario is typically characterized by a sequence of increasing periodicity, with a sudden transition to period 1 or period 2, as the control parameter Ω is changed.

In conclusion, we observed transitions from multiperiodic to single periodic bubbling regimes during the formation of sparkling bubbles. These bubbling transitions undergo a sequence known as a period-adding route, based on a model that takes into account the coupling between two dominating time scales: the bubbling frequency F_b and the frequency F_c of the gas pocket that oscillates while trapped inside the cellulose fiber's lumen. In our model, the distribution of periodic solutions follows a sequence of different bubbling regimes, and the transitions between these different bubbling regimes depends on the ratio of the two latter frequencies, i.e., the parameter $\Omega = F_c/F_b$.

[1] N. Shafer and R. Zare, Phys. Today **44**, 48 (1991).
[2] G. Liger-Belair, Sci. Am. **288**, 80 (2003).
[3] T. Clarke, Nature **409**, 554 (2001).
[4] W. Konrad and A. Roth-Nebelsick, J. Theor. Neurobiol. **224**, 43 (2003).
[5] A. B. Branger, C. J. Lambertsen, and D. M. Eckmann, J. Appl. Physiol. **90**, 593 (2001).
[6] S. Coombes and A. H. Osbaldestin, Phys. Rev. E **62**, 4057 (2000).
[7] L. Glass, Nature **410**, 277 (2001).
[8] Y. Hasegawa, K. Tanaka, and Y. Ueda, Int. J. Bifurcation Chaos Appl. Sci. Eng. **11**, 3003 (2001).
[9] G. Tanaka, S. Murashige, and K. Aihara, Int. J. Bifurcation Chaos Appl. Sci. Eng. **13**, 3409 (2003).
[10] V. S. M. Piassi, A. Tufaile, and J. C. Sartorelli, Chaos **14**, 477 (2004).
[11] S. F. Jones, G. M. Evans, and K. P. Galvin, Adv. Colloid Interface Sci. **80**, 51 (1999).
[12] G. Liger-Belair, M. Vignes-Adler, C. Voisin, B. Robillard, and P. Jeandet, Langmuir **18**, 1294 (2002).
[13] D. J. Tritton and C. Egdell, Phys. Fluids A **5**, 503 (1993).
[14] R. Mosdorf and M. Shoji, Chem. Eng. Sci. **58**, 3837 (2003).
[15] E. Colli, V. S. M. Piassi, A. Tufaile, and J. C. Sartorelli, Phys. Rev. E **70**, 066215 (2004).